




PHOTONICS Research

Highly efficient on-chip erbium–ytterbium co-doped lithium niobate waveguide amplifiers

YUQI ZHANG,¹  QIANG LUO,¹  DAHUI ZHENG,^{1,3} SHUOLIN WANG,² SHIGUO LIU,¹ HONGDE LIU,^{1,*} 
FANG BO,^{1,4} YONGFA KONG,^{1,5} AND JINGJUN XU,^{1,6}

¹MOE Key Laboratory of Weak-Light Nonlinear Photonics, TEDA Institute of Applied Physics and School of Physics, Nankai University, Tianjin 300457, China

²School of Science, Jiangsu University of Science and Technology, Zhenjiang 212100, China

³e-mail: dhzheng@nankai.edu.cn

⁴e-mail: bofang@nankai.edu.cn

⁵e-mail: kongyf@nankai.edu.cn

⁶e-mail: jjxu@nankai.edu.cn

*Corresponding author: liuhd97@nankai.edu.cn

Received 14 June 2023; revised 27 July 2023; accepted 30 July 2023; posted 31 July 2023 (Doc. ID 497947); published 28 September 2023

The ability to amplify optical signals is of paramount importance in photonic integrated circuits (PICs). Recently, lithium niobate on insulator (LNOI) has attracted increasing interest as an emerging PIC platform. However, the shortage of efficient active devices on the LNOI platform limits the development of optical amplification. Here, we report an efficient waveguide amplifier based on erbium and ytterbium co-doped LNOI by using electron beam lithography and an inductively coupled plasma reactive ion etching process. We have demonstrated that signal amplification emerges at a low pump power of 0.1 mW, and the net internal gain in the communication band is 16.52 dB/cm under pumping of a 974 nm continuous laser. Benefiting from the efficient pumping facilitated by energy transfer between ytterbium and erbium ions, an internal conversion efficiency of 10% has been achieved, which is currently the most efficient waveguide amplifier under unidirectional pumping reported on the LNOI platform, to our knowledge. This work proposes an efficient active device for LNOI integrated optical systems that may become an important fundamental component of future lithium niobate photonic integration platforms. © 2023 Chinese Laser Press

<https://doi.org/10.1364/PRJ.497947>

1. INTRODUCTION

The ability to amplify optical signals holds vital importance in the fields of science and technology. Typically, signal amplification is achieved using rare-earth doped optical fibers or gain media based on III–V semiconductors [1]. An erbium (Er) doped fiber amplifier exhibits characteristics such as low nonlinearity and low noise amplification, which can cover the wide gain of C-band and L-band of telecommunications. It is the basis of the current long-distance optical fiber optical wave system. Compared with III–V semiconductors, rare-earth ions doped materials have the advantages of longer excited state lifetimes and less refractive index change caused by doped ion excitation, which promotes in-depth research on the photonic integrated circuits (PICs) of Er³⁺ doped waveguide amplifiers and lasers with various passive components on a chip-scale platform [2].

Lithium niobate (LiNbO₃, LN) is considered one of the most promising photonic materials due to its excellent electro-, nonlinear- and acousto-optic properties, as well as its

wide transparent window and relatively high refractive index [3,4]. LN on insulator (LNOI) has strong optical constraints and retains good bulk characteristics, making it the main thin film platform for building chip integrated devices [5–8]. In the past few years, significant advancements have been made in the development of frequency comb sources [9,10], electro-optic modulators [11,12], frequency converters [13], and photodetectors [14] based on the LNOI platform. However, due to the indirect bandgap structure of LN, it is difficult to achieve active optical gain, an important function in PICs. A promising solution for developing active devices based on LNOI is to dope rare-earth ions into LN. In recent years, significant progress has been made in the integration of active components such as amplifiers [15–19] and lasers [20–26] based on the Er³⁺ doped LNOI platform, demonstrating the enormous potential for achieving high-performance scalable light sources on the LNOI platform.

Considering the relatively weak pump absorption caused by the small absorption cross section of Er³⁺ at 980 nm, co-doping with ytterbium (Yb³⁺) with a larger absorption cross

section can effectively enhance the pump absorption at 980 nm [2,27]. When Yb^{3+} combines with Er^{3+} in the same host, the excited Yb^{3+} can transfer its energy to adjacent Er^{3+} , improving pump efficiency [28–30]. To date, an $\text{Er}^{3+}/\text{Yb}^{3+}$ co-doped amplifier has not been demonstrated on the LNOI platform.

In this paper, $\text{Er}^{3+}/\text{Yb}^{3+}$ co-doped LNOI waveguide amplifiers are first fabricated by electron beam lithography (EBL) and inductively coupled plasma reactive ion etching (ICP-RIE) processes. A 5 mm $\text{Er}^{3+}/\text{Yb}^{3+}$ co-doped waveguide amplifier has a net internal gain of 16.52 dB/cm at a signal wavelength of 1531 nm, and a power conversion efficiency of up to 10% between 980 and 1550 nm, representing the highest value with unidirectional pumping among Er^{3+} doped LNOI waveguide amplifiers to date. Furthermore, by analyzing the material properties of $\text{Er}^{3+}/\text{Yb}^{3+}$ co-doped, Er^{3+} doped, and Yb^{3+} doped LN crystals, the effect and advantages of co-doping are clarified.

2. FABRICATION

Fabrication of the $\text{Er}^{3+}/\text{Yb}^{3+}$ co-doped LNOI waveguide amplifiers starts from a Z-cut LNOI wafer that was ion-sliced from an $\text{Er}^{3+}/\text{Yb}^{3+}$ co-doped LN crystal grown by the Czochralski method. The preparation process is mainly divided into six steps, as shown in Fig. 1. First, an LN boule with a doping concentration (mole fraction) of 0.6% Er and 1.0% Yb was cut into wafers. Second, LNOI wafers were prepared using “smart-cut” technology in cooperation with NanoLN. The thicknesses of the $\text{Er}^{3+}/\text{Yb}^{3+}$ co-doped LN (LN:Er,Yb), silicon-dioxide buffer layer, and silicon substrate are 0.6, 2.0, and 500 μm , respectively. Then a layer of hydrogen silsesquioxane (HSQ) was spin-coated on the wafer. Subsequently, the waveguide mask was patterned by EBL. Next, an ICP-RIE machine with argon plasma etching was used to transfer the mask patterns into the $\text{Er}^{3+}/\text{Yb}^{3+}$ co-doped LN film, resulting in ridge waveguides with a 400 nm etching depth and 60° wedge angle. Then, the chip was immersed in a buffered oxide etchant (BOE) solution for 5 min to remove the residual resist mask. Last, the chip facets were cleaved mechanically to ensure efficient fiber-to-chip coupling.

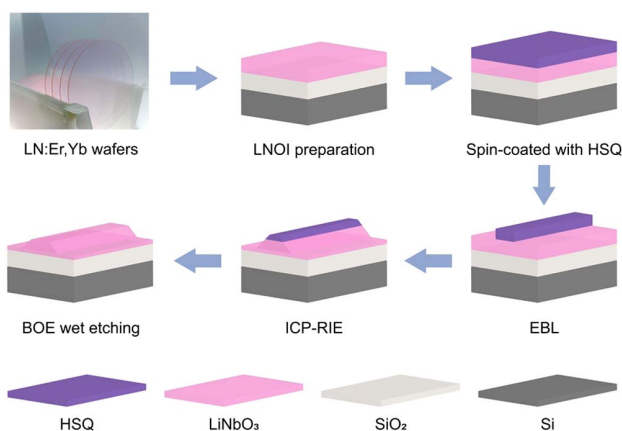


Fig. 1. Schematic of the fabrication process for $\text{Er}^{3+}/\text{Yb}^{3+}$ co-doped LNOI waveguides.

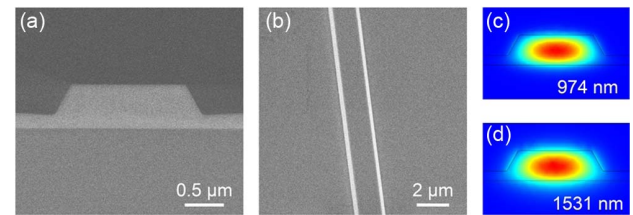


Fig. 2. SEM images of the (a) cross section and (b) longitudinal section of $\text{Er}^{3+}/\text{Yb}^{3+}$ co-doped LN waveguide. Simulated electric field distribution of single mode in the LN waveguide at (c) $\lambda = 974$ nm and (d) $\lambda = 1531$ nm.

Figures 2(a) and 2(b) present scanning electron microscope (SEM) images of the cross section and longitudinal section of the fabricated $\text{Er}^{3+}/\text{Yb}^{3+}$ co-doped LN waveguide. The final length and top width of the straight waveguide are about 5 mm and 1.5 μm , respectively. Based on the structural parameters of the waveguide, we calculated the mode distribution of the basic transverse electrical modes at the pump (~ 974 nm) and signal (~ 1531 nm) wavelengths, as shown in Figs. 2(c) and 2(d). The micrometer level ridge shaped LNOI waveguide has a high refractive index contrast, resulting in light field limitations in both the 980 and 1550 nm bands.

3. CHARACTERIZATION

The experimental setup shown in Fig. 3 was used to investigate the optical amplification performance of the $\text{Er}^{3+}/\text{Yb}^{3+}$ co-doped LNOI waveguides. A continuous laser at 974 nm and a continuous-wave C-band tunable laser operating in the 1550 nm band were selected as the pump and signal, respectively. Before the pump and signal were launched into the chip, a variable optical attenuator (VOA), optical coupler (OC), and polarization controller (PC) were connected into the optical path to adjust the pump and signal power, split the light into two paths, and optimize the polarization state with as much energy as possible in the TE fundamental mode in the waveguide, respectively. The pump and signal were combined by a wavelength division multiplexer (WDM) and launched into the $\text{Er}^{3+}/\text{Yb}^{3+}$ co-doped LNOI waveguide via a lensed fiber.

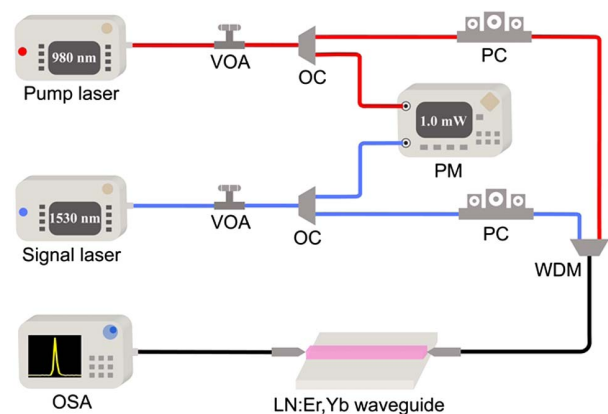


Fig. 3. Schematic of the experimental setup for characterization of $\text{Er}^{3+}/\text{Yb}^{3+}$ co-doped LNOI waveguide amplifiers.

Then, the amplified signal from the chip output facet was collected through a lensed fiber and emitted into an optical spectrum analyzer (OSA) to detect the optical amplification performance of the LNOI waveguide. Simultaneously, the pump/signal powers sent from the second port of OC were monitored by a power meter (PM).

Before characterizing the net internal gain of the $\text{Er}^{3+}/\text{Yb}^{3+}$ co-doped LN amplifier, we need to use the resonator Q -analysis method to characterize the pump light and signal light propagation losses of the waveguide. $\text{Er}^{3+}/\text{Yb}^{3+}$ co-doped LN microring resonators with a radius of $100\ \mu\text{m}$ were fabricated on the same chip in the same batch using the same waveguide parameters. As shown in Fig. 4, whispering-gallery modes at resonance wavelengths of 974 and 1531 nm were chosen for the measurement of the loaded Q factor by fitting the transmission curves with a Lorentz function, giving 2.03×10^5 and 1.43×10^5 loaded Q_L , respectively. According to the gap between the microring and waveguide, it was inferred that the 980 nm band was under-coupled and the 1550 nm band was over-coupled [31], so the intrinsic quality factors Q_i were 3.64×10^5 and 3.94×10^5 , respectively. The group index n_g at the relevant wavelength was calculated by $n_g = \lambda^2 / (2\pi R \cdot \text{FSR})$, where R and FSR are the microring radius and free spectral range. Consequently, the propagation loss coefficient α was estimated to be 1.85 dB/cm at 974 nm and 1.08 dB/cm at 1531 nm, according to

$$\alpha = \frac{2\pi n_g}{\lambda Q_i}. \quad (1)$$

It is worth noting that the propagation loss is mainly composed of waveguide scattering loss caused by sidewall roughness and absorption loss of Er and Yb ions. Considering the chip propagation loss and fiber-to-fiber insertion loss, we estimate that the fiber-to-chip coupling losses were 9.73 and 8.66 dB per facet at wavelengths of 974 and 1531 nm, respectively. The high coupling loss is caused by the unoptimized mode field distribution in LN waveguides and lensed fibers. Based on the above calibration results, this paper refers to the pump power and signal power as on-chip power.

The net internal gain of the $\text{Er}^{3+}/\text{Yb}^{3+}$ co-doped LN waveguide amplifier was obtained by

$$g = 10 \log_{10} \frac{P_{\text{on}}}{P_{\text{off}}} - \alpha L, \quad (2)$$

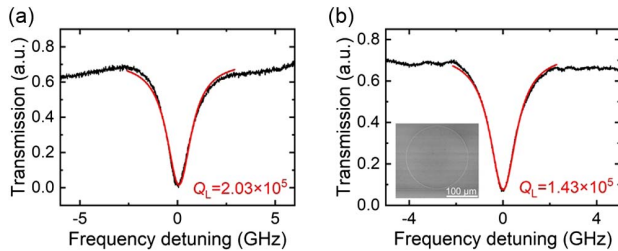


Fig. 4. Optical transmission spectra of $\text{Er}^{3+}/\text{Yb}^{3+}$ co-doped LNOI microring resonators on the same chip in (a) 980 nm band and (b) 1550 nm band. The Lorentz fit (red line) shows 2.03×10^5 and 1.43×10^5 loaded quality factors near 974 and 1531 nm, respectively. (The inset shows the SEM image of a microring resonator with a radius of $100\ \mu\text{m}$ used for testing in the 1550 nm band.)

in which P_{on} and P_{off} denote the output signal power in pump-on and pump-off cases with coupling loss deducted, and α and L respectively represent propagation loss at the signal wavelength and waveguide length. Therefore, αL is estimated as 0.54 dB.

Figure 5(a) shows the evolution of the measured signal spectrum with an increase of pump power at a fixed signal power. The dependence of net internal gain on the pump power of the integrated amplifier with a fixed signal power $\sim 28\ \text{nW}$ at 1531.3 nm is shown in Fig. 5(b). It can be observed that the signal begins to be amplified at a lower pump power ($\sim 0.1\ \text{mW}$). The initial net internal gain rapidly increases with pump power. Subsequently, when the pump power is greater than $1\ \text{mW}$, the net gain tends to saturate. Continue to increase the pump power, and the net internal gain remains stable. A maximum net internal gain of 6.87 dB is achieved at a pump power of 6.20 mW, corresponding to a net gain per unit length of 13.74 dB/cm. Compared to Er^{3+} doped LN straight waveguide amplifiers of the same length, the net internal gain is significantly improved at a low signal optical power.

In addition, we characterized the gain dependence of the waveguide amplifier on the signal power, as shown in Fig. 5(c). The fixed pump power is 6.20 mW, and the signal power is adjusted from -48 to $-7\ \text{dBm}$. When the signal power is approximately $-48\ \text{dBm}$, the maximum net internal gain is $\sim 8.26\ \text{dB}$ (16.52 dB/cm). Notably, with the increase of signal power, gain saturation can be observed, which is due to the depletion of the excited state population of Er ions. On this basis, we further estimated the internal conversion efficiency η of the $\text{Er}^{3+}/\text{Yb}^{3+}$ co-doped LN waveguide amplifier by the following equation [16]:

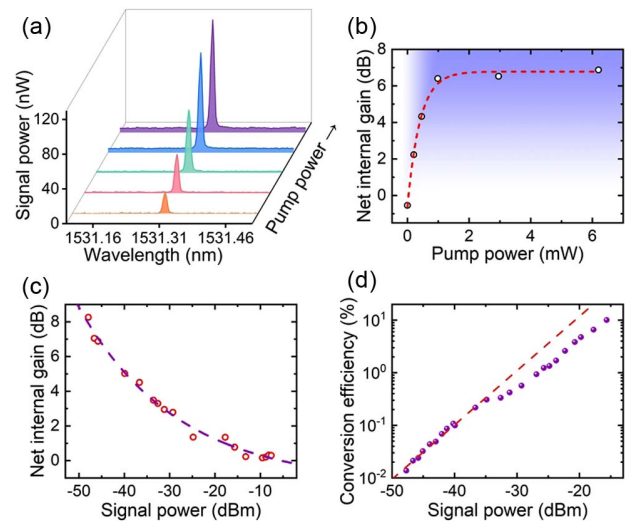


Fig. 5. (a) Measured signal spectra at $\sim 1531.31\ \text{nm}$ with increasing pump powers of 0, 0.21, 0.46, 2.96, and 6.20 mW. (b) Dependence of net internal gain on pump power at a fixed on-chip input signal power of $\sim 28\ \text{nW}$. (c) Net internal gain as a function of increasing signal power at a fixed pump power of $\sim 6.20\ \text{mW}$. (d) The measured internal conversion efficiency (purple dot) is used as a function of signal power. The red dashed line shows a linear trend based on small signal gain.

$$\eta = \frac{P_{\text{on}} - P_{\text{off}}}{P_{\text{pump}}} \times 100\%, \quad (3)$$

where P_{pump} is on-chip input power with coupling loss deducted. As depicted in Fig. 5(d), the measured conversion efficiency increases linearly with signal power in the small signal regime, and then gradually deviates from the linear trend as the signal optical power increases. At a maximum signal power of -15 dBm, the internal conversion efficiency reached 10%. The internal conversion efficiency is currently the highest reported value for on-chip Er^{3+} doped LNOI waveguide amplifiers. This result is mainly due to the co-doping of Yb^{3+} , which improves pump efficiency through energy transfer.

To study the superiority of 0.6% Er^{3+} and 1.0% Yb^{3+} co-doped LN (LN:Er,Yb), we grew 0.6% Er^{3+} doped LN (LN:Er) and 1.0% Yb^{3+} doped LN (LN:Yb) by the Czochralski method and used Z-cut wafers for exploration. Figure 6(a) shows the infrared absorption spectra of LN:Er,Yb, LN:Er, and LN:Yb by infrared absorption spectrometry. It can be clearly seen that the absorption band of LN:Er,Yb is the superposition of the absorption bands of LN:Er and LN:Yb, which can be excited over a wider range and has higher absorption in the 980 nm band, resulting in higher pump efficiency. Figure 6(b) shows the infrared photoluminescence (PL) emission spectra of LN:Er,Yb, LN:Er, and LN:Yb under 980 nm excitation at high pump power. It can be observed that the peaks of LN:Er and LN:Yb are at 1531 and 1062 nm, respectively. At this point, the peaks of LN:Er,Yb are close to LN:Er in the 1550 nm band. However, at lower pump power, the peaks of LN:Er,Yb are much higher as shown in the illustration. It indicates that the co-doping of Yb^{3+} enormously improves the pump efficiency.

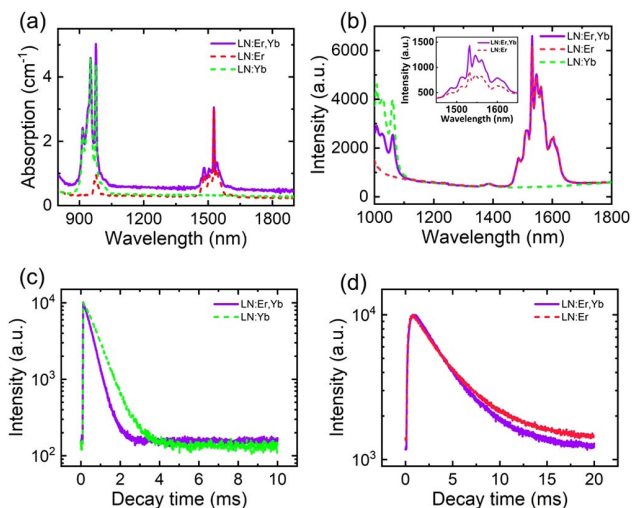


Fig. 6. (a) Infrared absorption spectra of $\text{Er}^{3+}/\text{Yb}^{3+}$ co-doped, Er^{3+} doped, and Yb^{3+} doped LN. (b) Infrared emission spectra of $\text{Er}^{3+}/\text{Yb}^{3+}$ co-doped, Er^{3+} doped, and Yb^{3+} doped LN under 980 nm excitation at high pump power. The inset shows the infrared emission spectra of $\text{Er}^{3+}/\text{Yb}^{3+}$ co-doped and Er^{3+} doped LN at lower pump power. (c) Decay curves of the Yb^{3+} emission at 1062 nm in $\text{Er}^{3+}/\text{Yb}^{3+}$ co-doped and Yb^{3+} doped LN, excited under 980 nm. (d) Decay curves of the Er^{3+} emission at 1531 nm in $\text{Er}^{3+}/\text{Yb}^{3+}$ co-doped and Er^{3+} doped LN, excited under 980 nm.

The decay behavior of LN:Er,Yb and LN:Yb transitions measured by a time-correlated single-photon counting method at Yb^{3+} ($\lambda_{\text{ex}} = 980$ nm) at 1062 nm is shown in Fig. 6(c). All attenuation curves can be well fitted by a function of time $I(t) = Ae^{-t/\tau}$, where A denotes the fitting amplitude, and τ represents decay time. The emission decay times of Yb^{3+} in LN:Er,Yb and LN:Yb are 0.40 and 0.64 ms, respectively. Energy transfer leads to faster decay of $\text{Er}^{3+}/\text{Yb}^{3+}$ co-doped LN, that is, the energy transfer to Er^{3+} constitutes an additional decay channel of Yb^{3+} in its excited state. Based on this, we estimated the energy transfer efficiency from Yb^{3+} to Er^{3+} by $E = 1 - \tau_{\text{Er,Yb}}/\tau_{\text{Yb}}$ [32], where $\tau_{\text{Er,Yb}}$ and τ_{Yb} are the emission decay times of Yb^{3+} in LN:Er,Yb and LN:Yb, respectively. The energy transfer efficiency is approximately 37.5%, which makes pumping in the 980 nm band more efficient. The decay behavior of LN:Er,Yb and LN:Er transitions measured at Er^{3+} ($\lambda_{\text{ex}} = 980$ nm) at 1531 nm is shown in Fig. 6(d). Er^{3+} has emission decay times of 3.52 and 3.77 ms in LN:Er,Yb and LN:Er, respectively. $\text{Er}^{3+}/\text{Yb}^{3+}$ co-doping did not significantly change the lifetime of Er^{3+} . In our opinion, the reason may be that Yb^{3+} has a large absorption cross section, which can absorb more pump energy and then transfer it to Er^{3+} , so that more Er^{3+} ions are excited. Compared with the 980 nm pump directly excited Er^{3+} , the effect of co-doping Yb^{3+} is equivalent to increasing the pump power and hardly affects the lifetime of Er^{3+} .

4. CONCLUSIONS

In summary, we manufactured on-chip $\text{Er}^{3+}/\text{Yb}^{3+}$ co-doped LNOI waveguide amplifiers for the first time using EBL and ICP-RIE processes. Under pumping in the 980 nm band, the communication band amplifier achieved a maximum net internal gain of approximately 16.52 dB/cm in a 5 mm long waveguide amplifier. Due to the efficient pumping that promotes energy transfer between Yb and Er ions, the demonstrated amplifier can achieve signal amplification at a low pump power of 0.1 mW and has a high internal conversion efficiency of 10% under unidirectional pumping. Compared with Er^{3+} doped amplifiers, the internal conversion efficiency is greatly improved. By analyzing the material properties, it was confirmed that the energy transfer from Yb^{3+} to Er^{3+} in LN:Er,Yb resulted in higher pump efficiency in the 980 nm band. In addition, by further optimizing the co-doping concentration of Er and Yb ions to achieve higher gain, growing crystals with better optical uniformity to reduce material losses, and designing a more suitable waveguide geometry to allow for high-power amplification, it is expected that the $\text{Er}^{3+}/\text{Yb}^{3+}$ co-doped LNOI waveguide amplifier will exhibit better amplification performance.

Funding. National Key Research and Development Program of China (2019YFA0705000); National Natural Science Foundation of China (12034010, 12134007); Natural Science Foundation of Tianjin City (21JCQNJC00250, 21JCZDJC00300); Program for Changjiang Scholars and Innovative Research Team in University (IRT_13R29).

Disclosures. The authors declare no conflicts of interest.

Data Availability. Data underlying the results presented in this paper are not publicly available at this time but may be obtained from the authors upon reasonable request.

REFERENCES

1. J. Riemensberger, N. Kuznetsov, J. Liu, J. He, R. N. Wang, and T. J. Kippenberg, "A photonic integrated continuous-travelling-wave parametric amplifier," *Nature* **612**, 56–61 (2022).
2. J. D. B. Bradley and M. Pollnau, "Erbium-doped integrated waveguide amplifiers and lasers," *Laser Photonics Rev.* **5**, 368–403 (2011).
3. M. Kösters, B. Sturman, P. Werheit, D. Haertle, and K. Buse, "Optical cleaning of congruent lithium niobate crystals," *Nat. Photonics* **3**, 510–513 (2009).
4. S. Wang, Y. Shan, D. Zheng, S. Liu, F. Bo, H. Liu, Y. Kong, and J. Xu, "The real-time dynamic holographic display of LN:Bi,Mg crystals and defect-related electron mobility," *Opto-Electron. Adv.* **5**, 210135 (2022).
5. J. Zhao, C. Ma, M. Rüsing, and S. Mookherjee, "High quality entangled photon pair generation in periodically poled thin-film lithium niobate waveguides," *Phys. Rev. Lett.* **124**, 163603 (2020).
6. Y. Kong, F. Bo, W. Wang, D. Zheng, H. Liu, G. Zhang, R. Rupp, and J. Xu, "Recent progress in lithium niobate: optical damage, defect simulation, and on-chip devices," *Adv. Mater.* **32**, 1806452 (2020).
7. D. Zhu, L. Shao, M. Yu, R. Cheng, B. Desiatov, C. J. Xin, Y. Hu, J. Holzgrafe, S. Ghosh, A. Shams-Ansari, E. Puma, N. Sinclair, C. Reimer, M. Zhang, and M. Lončar, "Integrated photonics on thin-film lithium niobate," *Adv. Opt. Photonics* **13**, 242–352 (2021).
8. A. Boes, L. Chang, C. Langrock, M. Yu, M. Zhang, Q. Lin, M. Lončar, M. Fejer, J. Bowers, and A. Mitchell, "Lithium niobate photonics: unlocking the electromagnetic spectrum," *Science* **379**, eabj4396 (2023).
9. L. Chang, S. Liu, and J. E. Bowers, "Integrated optical frequency comb technologies," *Nat. Photonics* **16**, 95–108 (2022).
10. C. Wang, M. Zhang, X. Chen, M. Bertrand, A. Shams-Ansari, S. Chandrasekhar, P. Winzer, and M. Lončar, "Integrated lithium niobate electro-optic modulators operating at CMOS-compatible voltages," *Nature* **562**, 101–104 (2018).
11. M. Zhang, C. Wang, P. Kharel, D. Zhu, and M. Lončar, "Integrated lithium niobate electro-optic modulators: when performance meets scalability," *Optica* **8**, 652–667 (2021).
12. S. Yuan, Y. Wu, Z. Dang, C. Zeng, X. Qi, G. Guo, X. Ren, and J. Xia, "Strongly enhanced second harmonic generation in a thin film lithium niobate heterostructure cavity," *Phys. Rev. Lett.* **127**, 153901 (2021).
13. M. Asgari, E. Riccardi, O. Balci, D. De Fazio, S. M. Shinde, J. Zhang, S. Mignuzzi, F. H. L. Koppens, A. C. Ferrari, L. Viti, and M. S. Vitiello, "Chip-scalable, room-temperature, zero-bias, graphene-based terahertz detectors with nanosecond response time," *ACS Nano* **15**, 17966–17976 (2021).
14. X. Sun, Y. Sheng, X. Gao, Y. Liu, F. Ren, Y. Tan, Z. Yang, Y. Jia, and F. Chen, "Self-powered lithium niobate thin-film photodetectors," *Small* **18**, 2203532 (2022).
15. J. Zhou, Y. Liang, Z. Liu, W. Chu, H. Zhang, D. Yin, Z. Fang, R. Wu, J. Zhang, W. Chen, Z. Wang, Y. Zhou, M. Wang, and Y. Cheng, "On-chip integrated waveguide amplifiers on erbium-doped thin-film lithium niobate on insulator," *Laser Photonics Rev.* **15**, 2100030 (2021).
16. Z. Chen, Q. Xu, K. Zhang, W.-H. Wong, D.-L. Zhang, E. Y.-B. Pun, and C. Wang, "Efficient erbium-doped thin-film lithium niobate waveguide amplifiers," *Opt. Lett.* **46**, 1161–1164 (2021).
17. Q. Luo, C. Yang, Z. Hao, R. Zhang, D. Zheng, F. Bo, Y. Kong, G. Zhang, and J. Xu, "On-chip erbium-doped lithium niobate waveguide amplifiers," *Chin. Opt. Lett.* **19**, 060008 (2021).
18. M. Cai, K. Wu, J. Xiang, Z. Xiao, T. Li, C. Li, and J. Chen, "Erbium-doped lithium niobate thin film waveguide amplifier with 16 dB internal net gain," *IEEE J. Sel. Top. Quantum Electron.* **28**, 8200608 (2022).
19. X. Yan, Y. Liu, J. Wu, Y. Chen, and X. Chen, "Integrated spiral waveguide amplifiers on erbium-doped thin-film lithium niobate," *arXiv*, arXiv:2105.00214 (2021).
20. Q. Luo, Z. Hao, C. Yang, R. Zhang, D. Zheng, S. Liu, H. Liu, F. Bo, Y. Kong, G. Zhang, and J. Xu, "Microdisk lasers on an erbium-doped lithium-niobate chip," *Sci. China Phys. Mech. Astron.* **64**, 234263 (2021).
21. Z. Wang, Z. Fang, Z. Liu, W. Chu, Y. Zhou, J. Zhang, R. Wu, M. Wang, T. Lu, and Y. Cheng, "On-chip tunable microdisk laser fabricated on Er³⁺-doped lithium niobate on insulator," *Opt. Lett.* **46**, 380–383 (2021).
22. Y. Liu, X. Yan, J. Wu, B. Zhu, Y. Chen, and X. Chen, "On-chip erbium-doped lithium niobate microcavity laser," *Sci. China Phys. Mech. Astron.* **64**, 234262 (2021).
23. R. Gao, J. Guan, N. Yao, L. Deng, J. Lin, M. Wang, L. Qiao, Z. Wang, Y. Liang, Y. Zhou, and Y. Cheng, "On-chip ultra-narrow-linewidth single-mode microlaser on lithium niobate on insulator," *Opt. Lett.* **46**, 3131–3134 (2021).
24. Q. Luo, C. Yang, R. Zhang, Z. Hao, D. Zheng, H. Liu, X. Yu, F. Gao, F. Bo, Y. Kong, G. Zhang, and J. Xu, "On-chip erbium-doped lithium niobate microring lasers," *Opt. Lett.* **46**, 3275–3278 (2021).
25. R. Zhang, C. Yang, Z. Hao, D. Jia, Q. Luo, D. Zheng, H. Liu, X. Yu, F. Gao, F. Bo, Y. Kong, G. Zhang, and J. Xu, "Integrated lithium niobate single-mode lasers by the Vernier effect," *Sci. China Phys. Mech. Astron.* **64**, 294216 (2021).
26. T. Li, K. Wu, M. Cai, Z. Xiao, H. Zhang, C. Li, J. Xiang, Y. Huang, and J. Chen, "A single-frequency single-resonator laser on erbium-doped lithium niobate on insulator," *APL Photonics* **6**, 101301 (2021).
27. S. Taccheo, G. Della Valle, K. Ennser, G. Sorbello, and S. Jiang, "Transient insensitive all-fibre gain-clamped EDFA based on highly-doped Er:Yb-fibre," *Electron. Lett.* **42**, 594–595 (2006).
28. E. Cantelar, J. Sanz-García, and F. Cussó, "Growth of LiNbO₃ codoped with Er³⁺/Yb³⁺," *J. Crystal Growth* **205**, 196–201 (1999).
29. E. Cantelar, J. A. Muñoz, J. A. Sanz-García, and F. Cusso, "Yb³⁺ to Er³⁺ energy transfer in LiNbO₃," *J. Phys. Condens. Mater.* **10**, 8893–8903 (1998).
30. C. Strohhofer and A. Polman, "Absorption and emission spectroscopy in Er³⁺-Yb³⁺ doped aluminum oxide waveguides," *Opt. Mater.* **21**, 705–712 (2003).
31. C. Zou, F. Shu, F. Sun, Z. Gong, Z. Han, and G. Guo, "Theory of free space coupling to high-Q whispering gallery modes," *Opt. Express* **21**, 9982–9995 (2013).
32. J. Tisler, R. Reuter, A. Lämmle, F. Jelezko, G. Balasubramanian, P. R. Hemmer, F. Reinhard, and J. Wrachtrup, "Highly efficient FRET from a single nitrogen-vacancy center in nanodiamonds to a single organic molecule," *ACS Nano* **5**, 7893–7898 (2011).